Properties and Structure of Ultrafine Amorphous Fe-Ni-B Powder Obtained by Borohydride Reduction

J.-G. Zhang

Ultrafine amorphous Fe-Ni-B powders were prepared by borohydride reduction, and their properties and structure were investigated by extended x-ray absorption fine structure (EXAFS), x-ray photoelectron spectroscopy (XPS), small-angle x-ray scattering (SAXS), Mössbauer spectra, transmission electron microscopy (TEM), differential scanning calorimetry (DSC), etc. The SAXS results for $Fe_{48}Ni_{21}B_{31}$ powders reveal the particle size statistic distribution, which is 1.7 nm, 80%; 6.4 nm, 8%; and 15.3 nm, 12%. TEM micrographs demonstrate the aggregates with fractal dimension of 1.5. The short-range order parameters of $Fe_{48}Ni_{21}B_{31}$ powders are obtained from EXAFS measurement. The XPS studies reveal that the higher H_c values of the powder prepared at higher reaction temperature relate to the appearance of the satellite structure at about 715.6 eV, which is characteristic for iron oxides, FeO/Fe_xO. This new interesting finding has been explained by the lattice misfit on the interface between the matrix and oxides, based on EXAFS studies. The crystalline behavior and magnetic properties demonstrate that there is no significant difference in amorphous structure between the chemically synthesized powders and melt-spun ribbons. However, the reasonable prediction of difference of amorphous structure and its formation mechanism between them has been proved by the XPS depth profile of $Fe_{48}Ni_{21}B_{31}$ powders, exhibiting considerable surface enrichment of boron and nickel, and EXAFS studies, showing a stronger interaction between nearer neighbors in the powders.

1. Introduction

AMORPHOUS alloys have many interesting properties, such as their excellent electrical, magnetic, mechanical, and chemical properties (Ref 1). Recently new techniques to obtain amorphous state materials have been developed, one of which is the chemical reduction of the metal ions, dissolved in water, with an aqueous solution of an alkali-metal borohydride as the reducing agent (Ref 2). The ultrafine amorphous transition metal-boron (TM-B) alloy particles obtained by borohydride reduction have attracted wide attention of scientists and technologists for two reasons. First, as the structure and properties of amorphous solids depend on preparation procedures due to their thermodynamic nonequilibrium state, it is interesting to compare the structure and properties of amorphous particles produced by this chemical reduction with those of amorphous materials obtained by other techniques. Second, in addition to the amorphous state, another striking characteristic of the particle is its ultrafine morphology. The minimum diameter of the particle, approximately 1 nm, can be attained in carefully controlled conditions. Nanostructural materials have received considerable attention in the past few years because of their novel combinations of mechanical, physical, and magnetic properties (Ref 3-5). These ultrafine amorphous powders have been expected to be applied to powder metallurgy, magnetic recording, catalysis, and ferrofluids by taking advantage of the novel

J.-G. Zhang, Shanghai Iron & Steel Research Institute, 1001 Tai He Rood, Shanghai 200940, China.

physical and chemical properties resulting from their fine particle size and amorphous state.

The experimental investigations of properties and structure of ultrafine amorphous Fe-Ni-B powders, which have been performed in Shanghai Iron & Steel Research Institute in the past few years and parts of which have been presented at conferences (Ref 6-8), are reported and reviewed in this paper. Some new interesting results obtained recently are also shown here.

2. Experimental Procedure

Fe-Ni-B alloy powders were prepared by the reduction of aqueous solutions of $FeSO_4$ and $NiCl_2$ using aqueous solutions of $NaBH_4$ or KBH_4. The 0.1 mol/L metallic salt solutions of Fe + Ni with different ratios of $FeSO_4$ to $NiCl_2$ were prepared. Then a $NaBH_4$ or KBH_4 aqueous solution of 0.5 or 1.0 mol/L was added to the above metallic salt solutions with vigorous stirring. The temperatures were 293 and 313 K, respectively.

Table 1 Sample preparation conditions and their effects on magnetic properties for Fe-Ni-B powders

Sample No.	Sample preparation condition			Magnetic properties	
	Mixing composition, atomic ratio	$NaBH_4$, concentration, mol/L	Reaction temperature, K	M_s, (Am^2/kg)	H_c, (kA/m)
1	$Fe_{100}Ni_0$	1.0	293	151.0	35.8
2	$Fe_{70}Ni_{30}$	1.0	293	98.0	39.8
3	$Fe_{70}Ni_{30}$	0.5	293	96.0	31.8
4	$Fe_{70}Ni_{30}$	1.0	313	90.3	42.2
5	$Fe_{30}Ni_{70}$	1.0	293	36.8	30.2
6	$Fe_{15}Ni_{85}$	1.0	293	14.3	25.1
7	Fe_5Ni_{95}	1.0	293	5.9	15.9

Table 2 Binding energies of various elements in $Fe_{48}Ni_{21}B_{31}$ powders for different Ar sputtering times

| Ar sputtering time, s	Binding energies, eV						
	Fe 2P3/2		Ni 2P3/2		B 1s		
	Oxidized	Metallic	Oxidized	Metallic	Oxidized	Metallic	O 1s
0	710.9	707.4	856.5	853.0	192.6	188.3	531.9
240	710.6	707.3	856.5	853.0	192.7	188.4	532.0
480	710.6	707.3	856.5	853.1	192.8	188.4	532.0
720	710.5	707.4	856.6	853.1	192.9	188.4	532.1
1080	710.4	707.5	...	853.2	192.9	188.6	532.2
1680	710.4	707.4	...	853.2	192.9	188.6	532.3
2400	710.4	707.3	...	853.0	192.9	188.4	532.2

2θ (°)
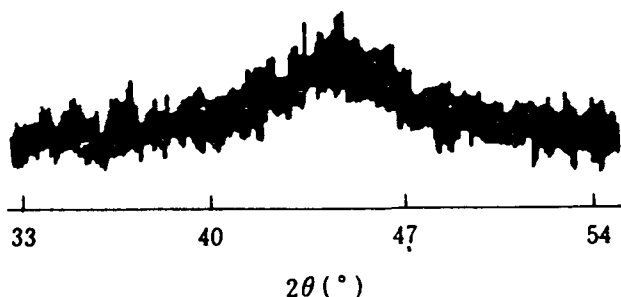
Fig. 1 X-ray diffractograph of $Fe_{48}Ni_{21}B_{31}$ powders.

After the reaction finished, the black product was immediately collected on a filter, washed, dried, and preserved in a desiccator. Table 1 summarizes the sample number and preparation conditions.

The chemical composition of the powder was determined by wet-chemical methods. Thermal analysis was carried out by DSC using Al_2O_3 as the reference material at a heating rate of 20 K/min. X-ray diffraction analysis was performed on a D-500 diffractometer using Cu $K\alpha$ radiation with 25 mA at 35 kV. Small-angle x-ray scattering was performed with a collimation system of four slits. The following experimental conditions were employed: Cu $K\alpha$ radiation; Ni filter; 55 kV; 180 mA; three slits S_1, S_2, and S_3 of 0.04, 0.03, and 0.05 mm, respectively; receiving slit of 0.1 mm; step scanning in a step of 0.02°; 40 s for each step; and scanning angle of 0.1 to 3°. The morphology of particle was observed with a Hitachi H-700 TEM (Hitachi, Ltd., Tokyo, Japan) at 200 kV. XPS was used for surface analysis, which was carried out on a VG instrument model MICROLAB MKII electron spectrometer (VG Scientific Ltd., Sussex, England) operated at a base pressure of 2×10^{-7} Pa. The Mg $K\alpha$ x-ray source (1253.6 eV) used here was operated at 15 kV and 20 mA. Compositional profiles were obtained by successive ion etching and analysis. The etching was performed in argon gas at 1×10^{-5} Pa with an argon ion gun operated at 3 kV and 0.8 µA. The Ni 2P3/2 line located at a binding energy (B.E.) value of 852.9 ± 0.1 eV was used as a reference in this work. The powder samples for surface analysis were prepared by lightly pressing the powders to form a 5-mm-diam disk. Mössbauer spectra were obtained by a constant-acceleration spectrometer with a 10 mCi (milliCuries) source of ^{57}Co in rhodium. A minicryogenerator was used to obtain cryogenic temperatures of ~10 K. The short-range structure of the powder was investigated by EXAFS. Its structure is compared with that

of an amorphous $Fe_{80}B_{20}$ ribbon. The measurements of x-ray absorption spectra were taken at the EXAFS station of synchrotron radiation in the Beijing Electron Positron Collider National Laboratory in the transmission mode with the storage ring operating at 2.2 GeV and an injection current of 39 mA. The energy range from 6900 to 9100 eV was scanned stepwise with a Si(111) double crystal monochromator. The smallest scanning step was 1 eV. The details of experimental procedure and data analysis of EXAFS investigation can be found elsewhere (Ref 9). Magnetic properties of the powders were measured with a model 155 vibrational sample magnetometer. The equilibrium time-constant of 3 seconds and maximum magnetic intensity of 1194 kA/m were used.

3. Experimental Results

3.1 Composition, Structure, and Morphology of the Powders

Chemical analysis of the powders shows that the atomic ratio between iron and nickel is identical with that in the original aqueous solution. Therefore, it is easy to control the ratio of iron to nickel in powders precisely. As an example, the chemical composition of sample 2 in Table 1 is 47.69 at.% Fe, 21.34 at.% Ni, and 30.97 at.% B (abbreviated to $Fe_{48}Ni_{21}B_{31}$ in the following).

Figure 1 demonstrates the XRD of $Fe_{48}Ni_{21}B_{31}$ powders, showing the amorphous state of the sample. The Mössbauer spectra of the powders described in section 3.4 also reveal the amorphous structure of the samples.

The crystallization behavior of the amorphous powders were investigated by thermal analysis. The DSC curves of $Fe_{48}Ni_{21}B_{31}$ show that the glass transition temperature (T_g) is 667 K, the onset crystallization temperature (T_x) is 693 K, and the peak crystallization temperature (T_p) is 716 K. These temperatures are comparable to the published data (Ref 10) of $T_x = 709$ K and $T_p = 743$ K for $Fe_{50.4}Ni_{21.8}B_{27.7}$.

The morphology of $Fe_{48}Ni_{21}B_{31}$ particles was observed by TEM (Fig. 2). In order to reveal the statistic distribution of particle size, SAXS was used to determine the volume fraction corresponding to different particle radii. The results for $Fe_{48}Ni_{21}B_{31}$ powders are (± 0.2 nm): 1.7 nm 80%, 6.4 nm 8%, and 15.3 nm 12%. The particles shown in Fig. 2 look larger than those derived from SAXS results. Figure 2 also exhibits the characteristics of fractal aggregates. The fractal dimension of the aggregates is 1.5.
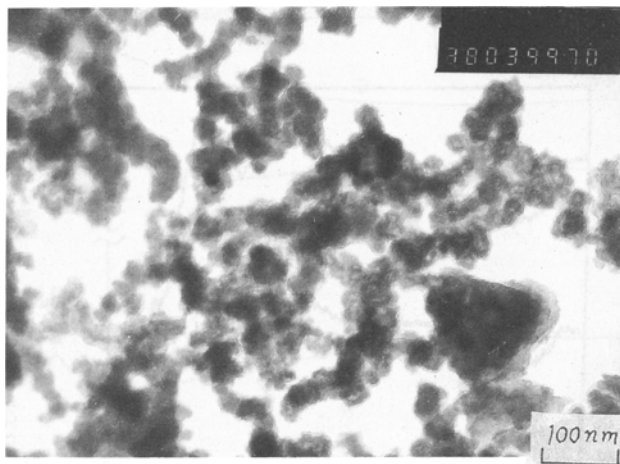
Fig. 2 TEM micrograph of $Fe_{48}Ni_{21}B_{31}$ ultrafine particles.

Fig. 3 XPS spectra of Ni, Fe, O, and B obtained from $Fe_{48}Ni_{21}B_{31}$ powders before (lower spectra) and after 20 min Ar sputtering (upper spectra).

3.2 XPS Surface Analysis

XPS spectra obtained from the surface of $Fe_{48}Ni_{21}B_{31}$ powders (sample No. 2) are illustrated in Fig. 3. They are recorded (a) shortly after sample transfer into the ultrahigh vacuum chamber ("as-received" state, the lower spectra) and (b) after Ar ion sputtering for 20 min (the upper spectra). Figure 4 presents XPS spectra obtained from sample No. 4, but only the Fe spectra in as-received and sputtered states are given for comparison with those in Fig. 3. Table 2 shows variation of the B.E. values during sputtering.

Two dominant peaks for Ni $2P_{3/2}$ are seen in Fig. 3. A peak of 853 eV B.E. is unambiguously due to metallic nickel. Another peak of 856.5 eV B.E. is due to oxidized nickel. The intensity of the oxidized Ni peak is higher than that of the metallic Ni peak in the as-received state, whereas the former is hardly seen and is much weaker than that of the latter after Ar sputtering for 20 min. The values of B.E. of metallic Ni $2P_{3/2}$ are within the experimental error the same as for the pure element in both the as-received and sputtered states. As shown in Table 2, the values of B.E. of oxidized Ni $2P_{3/2}$ are significantly shifted toward higher energy by 1.5 eV with reference to the B.E. value of 854.5 eV for NiO. A broad feature at about 862 eV B.E. appears in the as-received state and nearly disappears after 20 min Ar sputtering. The similar feature was also observed in the oxidized pure nickel sample as reported in the literature (Ref 11). The shift of B.E. and the broad feature do not allow an unambiguous assignment to a specific oxide and make it likely that different types of Ni species, e.g., NiO, Ni_2O_3, and $Ni(OH)_2$, are present.

Compared to metallic Ni $2P_{3/2}$, the very weak peak of metallic Fe $2P_{3/2}$ is found in the as-received state. The spectrum from the 20 min sputtered state demonstrates clearly the coexistence of the Fe $2P_{3/2}$ and Fe $2P_{1/2}$ peaks at 707.3 eV and 720.4 eV, respectively, which are characteristic for metallic iron. No significant differences of the values of B.E. of the metallic Fe $2P_{3/2}$ and Fe $2P_{1/2}$ are found in both the as-received and sputtered states as compared to the pure element. In contrast to the metallic Fe 2P peaks, the oxidized Fe $2P_{3/2}$ peak exhibits the shift of B.E. after Ar sputtering as is evident from Table 2. After 20 min sputtering, the oxidized Fe $2P_{3/2}$ level exhibits a small
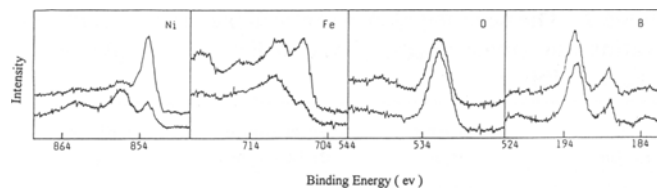
(0.5) but reproducible shift to lower binding energy, which could be related to the variation of the ratio of the various oxides. It was known that at least two different types of Fe oxides could be distinguished by their chemical shifts and satellite structures. For FeO and Fe_xO, a $2P_{3/2}$ peak at 709.6 eV and a satellite at 715.7 eV were reported (Ref 12), whereas for Fe_2O_3, Fe_3O_4, and FeOOH, Fe $2P_{3/2}$ peaks at about 711 eV and satellites at 719.7 eV were found (Ref 13). In the present work shown in Fig. 3, a weak shoulder at about 715.6 eV clearly appears after 20 min Ar sputtering, but it is hardly seen in the as-received state. On the other hand, a broad and weak feature around 720 eV, which is obscured by the overlapping Fe $2P_{1/2}$ peak, likely occurs in both the as-received and sputtered states. The above results of the B.E. shift of the oxidized Fe $2P_{3/2}$ peak and the appearance or disappearance of satellite structures indicate that both types of Fe oxides are present, whereas the intensity ratio of $Fe_2O_3/Fe_3O_4/FeOOH$ to FeO/Fe_xO decreases upon sputtering. As reported in the literature (Ref 14), the presence of FeOOH was corroborated by the observation that a green gel sheetlike net found in the formation of primary particles was identified as FeOOH.

The oxygen spectra shown in Fig. 3 reveal two features, the O lower spectra (1s) level at 531.9 eV and a broad hump at about 539 eV. Note the peak position of the spectra. While the O 1s peak position of the dry oxide layer is nearly constant at 530.1 eV, as expected for transition metal oxides (Ref 15), there are deviations from this value in both the as-received and sputtered states. The O 1s peak position for the spectrum from the as-received state is 531.9 eV and thus apparently higher than that for the dry oxide layer. This means that the oxide layer also contains species with higher binding energy, e.g., hydroxide and boron oxide, which are compatible with peaks at about 531 to 532 eV (Ref 16). Hydroxide appears to be likely because the powders are produced in aqueous solutions and, as indicated above, the iron spectra reveal the occurrence of FeOOH. Also, the presence of boron oxides is confirmed by the oxidized B 1s as discussed below. The spectra obtained after 20 min sputtering show a small peak shift from 531.9 to 532.2 eV, indicating an increase of relative amount of oxygen species with higher binding energy. The broad hump at about 539 eV is due to a Ni $L_3 M_{2,3}M_{2,3}$ Auger peak, which appears in the sputtered state and nearly disappears in the as-received state in Ni-containing samples, but has not been observed in Ni-free samples proving that this structure is associated with the presence of metallic nickel.

Two major peaks at 188.3 and 192.6 eV and two broad and weak structures at about 183 and 199 eV can be distinguished in the B 1s spectra of Fig. 3. The B.E. value of 188.3 eV due to

Table 3 The near neighbor structural parameters of the ultrafine amorphous $Fe_{48}Ni_{21}B_{31}$ powder and amorphous $Fe_{80}B_{20}$ ribbon

Sample	Central atom	Interatomic distance, nm	Coordination No.
$Fe_{48}Ni_{21}B_{31}$	Fe	0.230 ± 0.003	1.8 ± 0.4
		0.245 ± 0.002	6.0 ± 0.5
		0.264 ± 0.003	2.0 ± 0.4
	Ni	0.226 ± 0.004	4.0 ± 0.5
		0.242 ± 0.003	4.4 ± 0.3
		0.260 ± 0.003	1.2 ± 0.3
$Fe_{80}B_{20}$	Fe	0.239 ± 0.004	4.8 ± 0.4
		0.249 ± 0.003	3.9 ± 0.3
		0.278 ± 0.004	2.6 ± 0.4

Fig. 4 XPS spectra of Fe obtained from $Fe_{48}Ni_{21}B_{31}$ powders prepared at 313 K. For other conditions, see Fig. 3.

the metallic B 1s peak is in good agreement with the reported B.E. value of 188.0 eV in the $Ni_{81}Cr_{15}B_4$ sample (Ref 17), but it is higher than that of 187.5 eV in the pure element. For the oxidized state, compare the B.E. value of 192.6 eV due to the oxidized B 1s peak shown in Fig. 3 with the B.E. values of 191.1 eV in borides, 191.6 eV in the oxidized state of the pure element, and 193.5 eV in B_2O_3. The oxidized B 1s peak slightly shifts from 192.6 eV in the as-received state to 192.9 eV after 20 min sputtering as indicated in Table 2, which suggests that different types of boron oxides are present, and the relative intensity of the boron species with higher binding energy increases upon sputtering. The broad structures at about 183 and 199 eV are most likely attributed to the Cl species, the presence of which is proved by our secondary ion mass spectroscopy (SIMS) observation.

Figure 5 exhibits an XPS depth profile of $Fe_{48}Ni_{21}B_{31}$ powders. The intensities of the metallic and oxidized Ni $2P_{3/2}$ peaks increase and decrease rapidly upon sputtering, respectively, and the oxidized Ni $2P_{3/2}$ peak nearly disappears after Ar sputtering for 20 min. In contrast to Ni, the intensity of the oxidized Fe $2P_{3/2}$ peak decreases rather slowly upon sputtering, although the intensities of the metallic and oxidized Fe $2P_{3/2}$ peaks change upon sputtering in the same trend as those of Ni. A comparison of the depth distribution between Fe and Ni suggests that the thickness values of the oxide layers obtained from the data for Fe are significantly larger than those derived from the data for Ni. Hence, nickel reacts with oxygen more slowly than iron, and some metallic Ni remains in the oxide layer. The intensity of the O 1s peak apparently decreases upon sputtering, whereas only small changes of intensities of the B 1s peaks for both the metallic and oxidized states can be found during sputtering.

Although the data of quantitative analysis are not available in the present work in view of the fact that quantitative analysis is one of the most difficult and most inaccurate tasks in surface investigations, the changes of XPS relative intensities of the various elements illustrated in Fig. 5 do reveal interesting information about the mechanism of formation of amorphous powders as discussed in section 4.

3.3 EXAFS Measurement

The short-range order parameters obtained from EXAFS are listed in Table 3. The EXAFS data are used to elucidate the
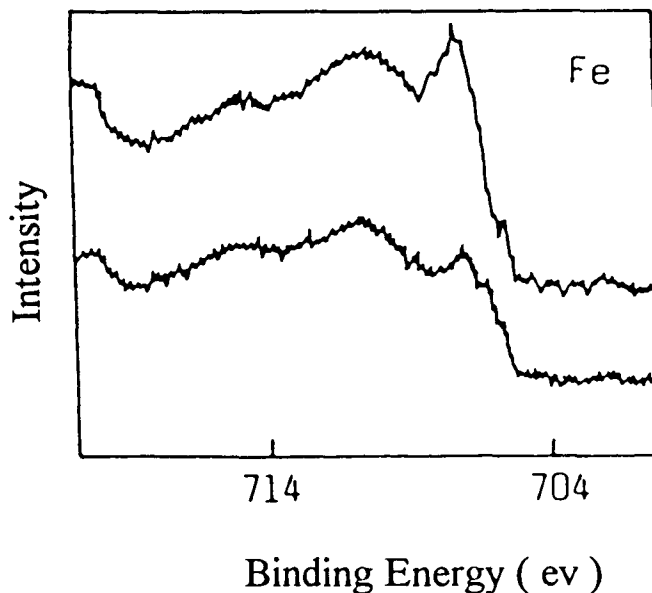
effect of reduction temperature on magnetic properties of the powders and to make a comparison among amorphous structures produced by chemical reduction and other methods, as discussed in section 4.

3.4 Mössbauer Spectra

Mössbauer spectroscopy has appeared to be very useful for the investigation on magnetic properties and atomic environments in amorphous systems. Figure 6(a) demonstrates Mössbauer spectrum of $Fe_{48}Ni_{21}B_{31}$ powders at room temperature, showing the amorphous state of the sample. Figure 6(b) and (c) show Mössbauer spectra of sample 5 at room temperature and 10 K, respectively. Figure 6(c) clearly demonstrates a decrease of a paramagnetic doublet and an increase of magnetic splitting in the central part of the spectrum. The paramagnetic doublet does not disappear completely even at 10 K. This fact can be explained by oxidation of powder surfaces, as proved in section 3.2.

3.5 Magnetic Properties

The values of saturation magnetization, M_s, and coercivity, H_c, of the powder samples are also shown in Table 1. The dependence of magnetic properties of the Fe-Ni-B powders on mixing metallic ion ratio (Ni/(Fe + Ni)) is illustrated in Fig. 7. As shown in Table 1, the M_s values of the powders are small compared to those for bulk samples, while the H_c values are apparently higher than those of bulk samples.

A comparison of the magnetic properties of the Fe-Ni-B powders obtained in the present work with those published in
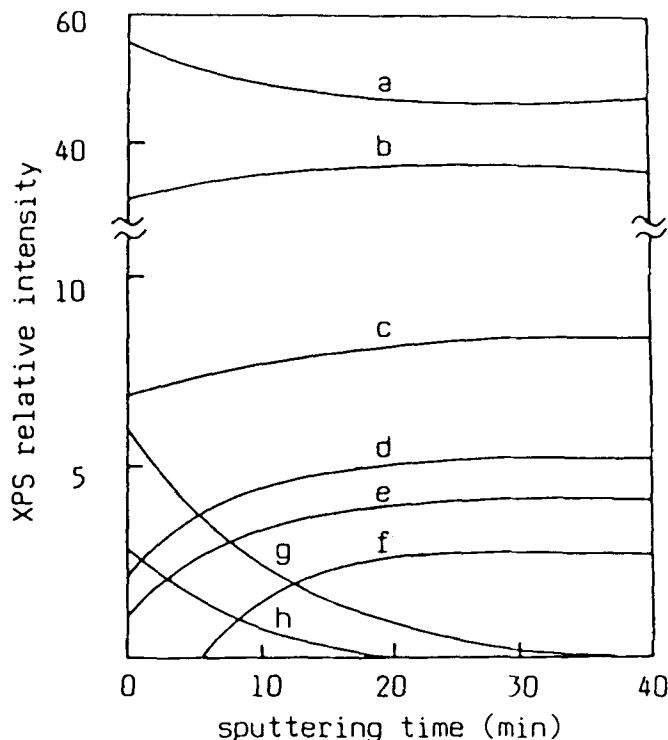
Fig. 5 XPS depth profile of $Fe_{48}Ni_{21}B_{31}$ powders. (a) O 1s. (b) B 1s (oxidized state). (c) B 1s (metallic state). (d) Ni $2P_{3/2}$ (metallic state). (e) Fe $2P_{3/2}$ (metallic state). (f) O (539 eV). (g) Fe $2P_{3/2}$ (oxidized state). (h) Ni $2P_{3/2}$ (oxidized state).
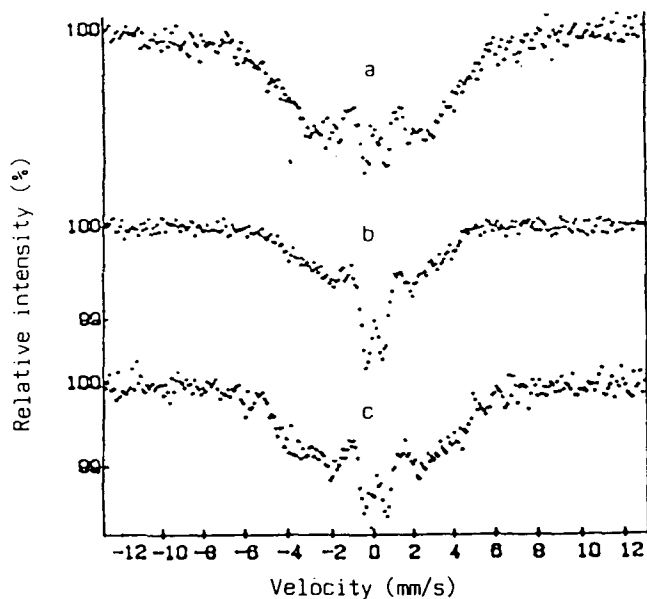

Fig. 6 Mössbauer spectra of Fe-Ni-B powders. (a) Sample 2 at room temperature. (b) Sample 5 at room temperature. (c) Sample 5 at 10 K.

Ref 18 indicates that the compositional dependence of M_s for both cases is similar, whereas the absolute values of M_s and H_c in the present work are apparently higher than those in Ref 18.

With a view to applications, the powders of higher values of M_s and H_c have more potential for commercialization. Also, by adjusting preparation conditions, crystalline Fe-Ni-B powder can be obtained, which has higher values of M_s and lower values of H_c than those of amorphous powders, respectively. Therefore, different magnetic properties of Fe-Ni-B powders produced by chemical reduction can be obtained by the alternative of amorphous state or crystalline one and by changing particle size and composition of powders in order to meet a wide variety of applications.

4. Discussion
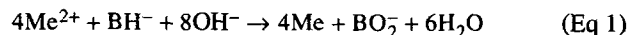
4.1 Effect of Reduction Conditions on Magnetic Properties

Because magnetic properties are of great importance to both theoretical interest and practical applications, they are discussed in more detail.

4.1.1 Effect of Mixing Metallic Ion Ratio

As shown in Fig. 7, the magnetization of the powders varies linearly with atomic concentration ratio of Ni/(Fe + Ni).

4.1.2 Effect of Concentration of Borohydride

The effect of concentration of $NaBH_4$ on magnetic properties can be found by comparing samples 2 and 3. To elucidate, it must be determined if there is a significant change in the reaction mechanism with concentration of borohydride. Saida et al. (Ref 19) proposed the following reactions in the chemical reduction with NaBH for (Fe,Co,Ni)-B alloys:

$$4Me^{2+} + BH^- + 8OH^- \rightarrow 4Me + BO_2^- + 6H_2O \qquad (Eq\ 1)$$

$$4Me^{2+} + 2BH_4^- + 6OH^- \rightarrow 2MeB + 6H_2O + H_2 \qquad (Eq\ 2)$$

where Me is Fe, Co, and Ni.

The H_c decreases monotonically with M_R ($M_R = M_{KBH_4}/M_{Metal}$), where M_{KBH_4} is the mol concentration of KBH_4 and M_{Metal} is that of metal ions, while the M_s remains almost constant in the Fe-B system due to a change in the reaction mechanism. In the present paper, when the concentration of $NaBH_4$ increased from 0.5 to 1.0 mol/L, corresponding to an increase of M_R from 5 to 10, the H_c increased, not decreased. This fact implies that there is no significant change in the reaction mechanism with M_R for the Fe-Ni-B powders. In the condition of same reaction mechanism, the higher reaction rate corresponding to the case of higher reactant concentration produces finer particle size, which in turn, results in a higher value of H_c.

4.1.3 Effect of Reaction Temperature

A comparison of samples 2 and 4 indicates that magnetization, M_s, decreases and coercivity, H_c, increases due to the higher reaction temperature. The higher reaction rate due to higher reaction temperature produces finer particle size, which in turn, results in a higher value of H_c. The severer oxidation of
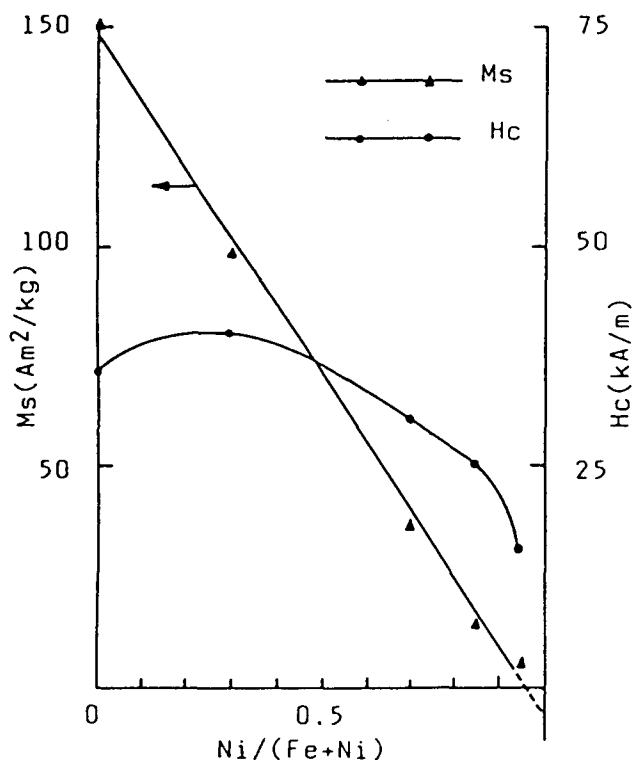
Fig. 7 The dependence of M_s and H_c on Ni/(Fe + Ni) for Fe-Ni-B powders.

5. Summary

The ultrafine amorphous Fe-Ni-B powders with different Fe/Ni ratios were prepared by borohydride reduction, and their properties and structure were investigated by EXAFS, XPS, SAXS, Mössbauer spectra, TEM, DSC, etc. The Fe/Ni ratios in the powders were found to be identical with those in aqueous solutions. XRD and Mössbauer spectra demonstrate the amorphous structure of the powders. The DSC measurement of $Fe_{48}Ni_{21}B_{31}$ powders shows that $T_g = 667$ K, $T_x = 693$ K, and $T_p = 716$ K. The SAXS results for $Fe_{48}Ni_{21}B_{31}$ powders reveal the particle size statistic distribution, which is 1.7 nm, 80%; 6.4 nm, 8%, and 15.3 nm, 12%. TEM micrographs demonstrate the aggregates with fractal dimension of 1.5. The XPS spectra of $Fe_{48}Ni_{21}B_{31}$ powders show that both metallic and oxidized peaks of Ni, Fe, and B are found. Two different types of Fe oxides, FeO/Fe_xO and $Fe_2O_3/Fe_3O_4/FeOOH$, can be distinguished by their chemical shifts and satellite structures. The presence of hydroxide is also supported by the oxygen spectra. The shifts of oxidized Ni and B peaks suggest that different types of nickel and boron oxides are present. Mössbauer studies exhibit the evidence for superparamagnetism in the high Ni content samples. The short-range order parameters of $Fe_{48}Ni_{21}B_{31}$ powders are obtained from EXAFS measurement. The magnetic properties measurement indicates the lower values of magnetization, M_s, and the much higher values of coercivity, H_c, of the powders as compared with those of the bulk samples. The magnetization, M_s, of the powders decreases linearly with increasing atomic concentration ratio of Ni/(Fe + Ni). A peak of coercivity H_c appears at the ratio Ni/(Fe + Ni) of 0.3. When the concentration of $NaBH_4$ increases from 0.5 to 1.0 mol/L, a higher H_c value of the powders is obtained. The XPS studies reveal that the higher values of H_c of the powders prepared at a higher reaction temperature relate to the appearance of the satellite structure at about 715.6 eV, which is characteristic for iron oxides, $FeO/Fe/_xO$. This new interesting finding has been explained by the lattice misfit on the interface between the matrix and oxides, based on EXAFS studies. The experimental data of crystallization behavior and magnetic properties demonstrate that there is no significant difference in amorphous structure between the chemically synthesized powders and melt-spun ribbons. The XPS depth profile of $Fe_{48}Ni_{21}B_{31}$ powders exhibits considerable surface enrichment of boron and nickel, suggesting that mechanism of formation of amorphous structure obtained by chemical reduction is different from that produced by rapid quench. The EXAFS measurement shows that the mean distance and coordination number of near neighbors around Fe and Ni in the powders are smaller than those in binary Fe-B and Ni-B amorphous ribbons of similar compositions.

particle surfaces at the higher reaction temperature for sample 4 may be the other source for the higher H_c value. This is also supported by the fact that the magnetization of sample 4 is lower than that of sample 2. Although this explanation is reasonable, it is only a phenomenological one, and knowledge of the details of the mechanism has not yet been provided.

A comparison of Fe spectra between samples 2 and 4 shown in Fig. 3 and 4, respectively, indicates that the higher H_c values are related to the presence of iron oxides, FeO/Fe_xO, but not iron species, $Fe_2O_3/Fe_3O_4/FeOOH$. Further, according to EXAFS studies shown in Table 3, a mechanism is provided to indicate that the higher H_c value of sample 4 is due to the higher value of stress at the interface between the matrix and FeO, which results from the structure similar to semicoherent interface (Ref 8).

4.2 The Amorphous Structure and its Formation Mechanism of the Powders

The XPS depth profile of $Fe_{48}Ni_{21}B_{31}$ powders reveals considerable surface enrichment of boron and nickel, indicating the difference between the amorphous structure obtained by chemical reduction and that produced by rapid quench. Another important difference is that there is a stronger interaction between near neighbors in the powders obtained by chemical reduction, which is based on EXAFS investigations (Ref 9).

References

1. T. Sato, Further Improvement of Core Loss in Amorphous Alloys, *J. Mater. Eng. Perform.*, Vol 2 (No. 2), 1993, p 235-240

2. J.V. Wonterghem, S. Mørup, C.J.W. Koch, S.W. Charles, and S. Wells, Formation of Ultra-Fine Amorphous Alloy Particles by Reduction in Aqueous Solution, *Nature*, Vol 322 (No. 6080), 1986, p 622-623

3. G. Herzer, On the Theoretical Understanding of Nanocrystalline Soft Magnetic Materials, *J. Mater. Eng. Perform.*, Vol 2 (No. 2), 1993, p 193-197

4. N. Hasegawa, M. Saito, N. Kataoka, and H. Fujimori, Soft Magnetic Properties of Carbide-Dispersed Nanocrystalline Films with High Thermal Stability, *J. Mater. Eng. Perform.*, Vol 2 (No. 2), 1993, p 181-192

5. H.A. Davies, A. Manaf, and P.Z. Zhang, Nanocrystallinity and Magnetic Property Enhancement in Melt-Spun Iron-Rare Earth-Base Hard Magnetic Alloys, *J. Mater. Eng. Perform.*, Vol 2 (No. 4), 1993, p 579-587

6. J.-G. Zhang, W. Mei, G. Xu, J. Jin, Y. Sun, X. Yang, B. Hu, J. Jiang, and X. Ru, Magnetic Properties and Mossbauer Spectroscopy Studies of Ultrafine Amorphous Fe-Ni-B Powders, *Proc. 2nd Int. Symp. Phys. Mag. Mater.*, Vol 2, S.G. Zhang, Ed., International Academic Publishers, 1992, p 589-592

7. J.-G. Zhang, W.X. Xu, Q. Zhang, G.Q. Lao, X.L. Yang, B.Y. Hu, and J.S. Jiang, XPS and Mossbauer Studies of Ultrafine Amorphous Fe-Ni-B Powder, *Proc. 1st Pacific Rim Int. Conf. Adv. Mater. Proc.*, C.X. Shi, H.D. Li, and A. Scott, Ed., TMS, 1993, p 393-398

8. J.-G. Zhang, W.X. Xu, Z.Q. Zhang, J. Zhn, W.C. Wang, and Y. Chen, The Effect of Reduction Condition on Properties of Ultrafine Amorphous Fe-Ni-B Powders Obtained by Borohydride Reduction, "Advanced Materials"—New Processes and Reliability, *Proc. 3rd Japan Int. SAMPE Symp.*, Vol 1, T. Kish, N. Takeda, and Y. Kagawa, Ed., Chiba, Japan, 1993, p 1064-1069

9. W.-C. Wang, Yu. Chen, J.-G. Zhang, and T.-D. Hu, Short-Range Order in Ultrafine Powder of an Amorphous $(Fe_7Ni_3)_{69}B_{31}$ Alloy, *J. Non-Cryst. Solids*, Vol 160 (No. 3), p 268-274

10. A. Inoue, J. Saida, and T. Masumoto, Formation of Ultra-Fine Amorphous Powders in Fe-M-B (M = Transition Metal) Systems by Chemical Reduction Method and Their Thermal and Magnetic Properties, *Metall. Trans. A*, Vol 19 (No. 9), 1988, p 2315-2318

11. N. Winograd, W.E. Baitinger, J.W. Amy, and J.A. Munarin, X-Ray Photoelectron Spectroscopic Studies of Interactions in Multicomponent Metal and Metal Oxides Thin Film, *Science*, Vol 184 (No. 4136), 1974, p 565-567

12. G. Grenet, Y. Jugnet, T.M. Duc, and M. Kibler, On the FeO Valence Band Photoemission Spectra, *J. Chem. Phys.*, Vol 72 (No. 1), 1980, p 218-220

13. C.R. Brundle, T.J. Chuang, and K. Wandelt, Core and Valence Level Photoemission Studies of Iron Oxide Surfaces and the Oxidation of Iron, *Surf. Sci.*, Vol 68, 1977, p 459-468

14. S.G. Kim and J.R. Brock, Growth of Ferromagnetic Particles from Cation Reduction by Borohydride Ions, *J. Colloid. Interface Sci.*, Vol 116 (No. 2), 1987, p 431-443

15. K. Wandelt, Photoemission Studies of Absorbed Oxygen and Oxide Layers, *Surf. Sci. Rep.*, Vol 2 (No. 1), 1982, p 1-121

16. Z. Zsoldos, Z. Schay, and L. Guczi, Oxygen-Containing Species on Amorphous $Fe_{80}B_{20}$ and $Fe_{40}Ni_{40}B_{20}$ Alloys During Chemisorption of CO and H_2, *Surf. Interface Anal.*, Vol 12 (No. 1-12), 1988, p 257-261

17. S.K. Kulkarni, M.G. Thube, and A.S. Nigavekar, Electronic-Structure Study of $Ni_{81}Cr_{15}B_4$ Metallic Glass Using Photoemission Spectroscopy, *Phys. Rev. B.*, Vol 37 (No. 12), 1988, p 6723-6730

18. J. Saida, A. Inoue, and T. Masumoto, Formation of Ultrafine Amorphous Powders in (Fe, Co, Ni)-B Systems by Chemical Reduction Method and Their Thermal and Magnetic Properties, *Sci. Rep. Res. Inst., Tohoku Univ. A*, Vol A-34 (No. 2), 1989, p 205-215

19. J. Saida, A. Inoue, and T. Masumoto, The Effect of Reduction Condition on Composition and Properties of Ultrafine Amorphous Powders in (Fe, Co, Ni)-B Systems Prepared by Chemical Reduction, *Metall. Trans. A*, Vol 22 (No. 9), 1991, p 2125-2132